Unsupervised change detection using fuzzy c-means and MRF from remotely sensed images

Ming Hao, Hua Zhang, Wenzhong Shi & Kazhong Deng

Taylor & Francis
Taylor & Francis Group

Unsupervised change detection using fuzzy *c*-means and MRF from remotely sensed images

MING HAO†, HUA ZHANG†, WENZHONG SHI*‡ and KAZHONG DENG†

†Jiangsu Key Laboratory of Resources and Environmental Information Engineering, China University of Mining and Technology, Xuzhou, China
‡Joint Research Laboratory on Spatial Information, The Hong Kong Polytechnic University and Wuhan University, Wuhan and Hong Kong, China

In this paper, a novel change detection approach is proposed using fuzzy *c*-means (FCM) and Markov random field (MRF). First, the initial change map and cluster (changed and unchanged) membership probability are generated through applying FCM to the difference image created by change vector analysis (CVA) method. Then, to reduce the over-smooth results in the traditional MRF, the spatial attraction model is integrated into the MRF to refine the initial change map. The adaptive weight is computed based on the cluster membership and distances between the centre pixel and its neighbourhood pixels instead of the equivalent value of the traditional MRF using the spatial attraction model. Finally, the refined change map is produced through the improved MRF model. Two experiments were carried and compared with some state-of-the-art unsupervised change detection methods to evaluate the effectiveness of the proposed approach. Experimental results indicate that FCMMRF obtains the highest accuracy among methods used in this paper, which confirms its effectiveness to change detection.

1. Introduction

In remote sensing, change detection aims to identify changes occurred on the Earth surface by analysing multitemporal images acquired on the same geographical area at different times (Coppin *et al.* 2004, Lu *et al.* 2004, Radke *et al.* 2005, Bruzzone and Bovolo 2013). Over the past few years, many change detection methods have been imposed for various remotely sensed data. Generally, these methods can be grouped into supervised (post-classification) and unsupervised types (Bruzzone and Prieto 2000, Yetgin 2012). Though the supervised change detection methods supply the land-cover transformation, unsupervised change detection methods are more widely used and researched, thanks to the limitations of classification accuracy and ground reference absence (Bruzzone and Prieto 2000, Bovolo *et al.* 2008).

In this paper, we focus on the unsupervised change detection. Unsupervised change detection could be seen as a clustering process to partition pixels into changed and unchanged parts using some methods, such as image differencing, image ratio, image regression, and change vector analysis (CVA), etc. (Yetgin 2012, Shi and Hao 2013). One of the most widely used change techniques is to analyse the difference image created by subtracting corresponding bands of the multitemporal images pixel by pixel. Some

---

*Corresponding author. Email: lswzshi@polyu.edu.hk

literatures proposed automatic analysis for the difference image instead of an empirical threshold to identify changes (Huang and Wang 1995, Bruzzone and Prieto 2000, Bazi *et al.* 2005, Im *et al.* 2008). Additionally some methods of pattern recognition or machine learning have also been applied to this issue like active contour model (Bazi *et al.* 2010), support vector machine (SVM) (Bovolo *et al.* 2008), wavelet transform (Bovolo and Bruzzone 2005, Celik and Ma 2010), fuzzy *c*-means (FCM) (Ghosh *et al.* 2011), and so on. Indeed, when FCM is used to detect changes, it is unreasonable to identify changes just using membership probability since the ranges of pixel values of the difference image belonging to the two clusters (changed and unchanged) generally have overlap (Ghosh *et al.* 2011). To reduce speckle noise of the change map, the spatial context information has also been utilized, for example, Markov random field (MRF) is a classic approach to exploit the context information (Bruzzone and Prieto 2000, Melgani and Bazi 2006, Liu *et al.* 2008, Moser and Serpico 2009, Marchesi *et al.* 2010, Wang *et al.* 2013). Though MRF is commonly robust in its change detection (or classification) performance, the resulting change map will eventually reveal an over-smooth result (i.e., loss of significant details and generating too large patches) without well defining for the boundary pixels (Wang and Wang 2004, Tso and Olsen 2005).

In this paper, a novel change detection approach is proposed using FCM and MRF to address, for example, the absence of detailed information of traditional MRF and the value overlap of changed and unchanged pixels in the difference image of FMC. As shown in figure 1, the proposed approach is made up of three blocks as follows. First, the difference image is generated using CVA method based on multi-temporal remotely sensed images. Then FCM is performed to the difference image, so the initial change map and the cluster membership probability of pixels belonging to changed and unchanged parts are obtained. Finally, the membership probability is introduced into MRF using the spatial attraction model to control the boundary pixels in this process and the change map is produced.

2. Proposed change detection approach

Let X_1 and X_2 be two multispectral images acquired in same geographical area at two different times. Since the focus is on the change detection process, it is assumed that the multitemporal images have been co-registered and radiometrically corrected
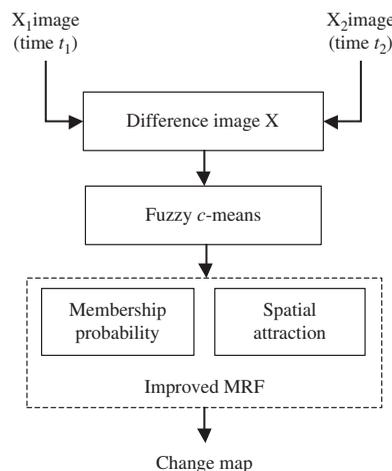

Figure 1. General scheme of the proposed approach.

and have the same size of $M_1 \times M_2$. Thus, the difference image $\mathbf{X}$ is generated by CVA method with the same size of $M_1 \times M_2$.

2.1. *Fuzzy* c-*means*

Suppose there are n pixels in the difference image $\mathbf{X} = \{x_1, x_2, ..., x_n\}$, and c is the number of the clusters. The FCM aims at obtaining membership probability $u_{ij} \in [0, 1]$ $\left(\sum_{i=1}^{c} u_{ij} = 1 \, (j = 1, 2, ..., n) \right)$ of the pixel x_j in the difference image for the ith cluster by minimizing the objective function

$$J(\mathbf{U}, \mathbf{V}) = \sum_{i=1}^{c} \sum_{j=1}^{n} u_{ij}^m \left\| x_j - v_i \right\|^2 \tag{1}$$

where $\mathbf{U} = [u_{ij}]$ is the membership probability matrix of $\mathbf{X}$, and $\mathbf{V} = [v_1, v_2, ..., v_c]$ is the matrix composed of c central values, each one containing the coordinates of a cluster centre. v_i is computed as follow

$$v_i = \frac{\sum_{j=1}^{n} u_{ij}^m x_j}{\sum_{j=1}^{n} u_{ij}^m} \tag{2}$$

where m is a weighting exponent and usually set to 2, a widely used value in many works. The membership probability u_{ij} is expressed as

$$u_{ij} = \frac{1}{\sum_{k=1}^{c} \left(\frac{\left\| x_j - v_i \right\|}{\left\| x_j - v_k \right\|} \right)^{\frac{2}{m-1}}} \tag{3}$$

In FCM we generally normalize the partition $\mathbf{U}$, with its elements falling within $[0, 1]$, and update $\mathbf{U}$ and $\mathbf{V}$ iteratively to approach an optimum solution. The iteration process is stopped when $\left\| \mathbf{V}_t - \mathbf{V}_{t-1} \right\| < \varepsilon$ is achieved, where $\mathbf{V}_t$ and $\mathbf{V}_{t-1}$ are the cluster centre matrix in the tth and $(t-1)$th iteration and ε is predefined threshold. Additionally, if the number of iterations oversteps a predefined maximum number, the iteration process is also stopped. More details about this can be found in Bezdek *et al.* (1984). Finally, the initial change map and the membership probability $\mathbf{U}$ of pixels in the difference image are both achieved.

2.2. *MRF incorporated the spatial attraction model*

Suppose the difference image $\mathbf{X} = \{x_1, x_2, ..., x_n\}$ is given, and $L = \{l_1, l_2, ..., l_c\}$ denotes the class label of the difference image and c is the number of classes. The Maximum a Posteriori (MAP) is adopted to produce the labels of pixels, and the formulation is described as

$$L = \arg \max \{ P(L) p(\mathbf{X}|L) \} \tag{4}$$

where $P(L)$ is a priori probability distribution of the class labels of the difference image, and $p(X|L)$ is the joint probability density function of the pixel values in the difference image. In terms of the MRF approach, maximizing the posterior probability as equation (4) is equivalent to minimize the following energy function $U_{MRF}(x_i)$ with a pixel x_i (Bruzzone and Prieto 2000, Tarabalka *et al.* 2010):

$$U_{MRF}(x_i) = U_{spectral}(x_i) + U_{spatial}(x_i) \tag{5}$$

where $U_{spectral}(x_i)$ describes the spectral energy function from the difference image and $U_{spatial}(x_i)$ represents the spatial energy term computed from the local neighbourhood N_i of the pixel x_i.

The detailed spectral energy term can be written as

$$U_{spectral}(x_i) = \frac{1}{2}\ln\left|2\pi\sigma_k^2\right| + \frac{1}{2}(x_i - \mu_k)^2(\sigma_k^2)^{-1} \tag{6}$$

here μ_k and σ_k^2 denote the mean and variance of class k, respectively, that can be calculated from the initial change map generated by FCM.

The spatial energy of the pixel x_i is defined as

$$U_{spatial}(x_i) = \beta \sum_{j \in N_i} I(l(x_i), l(x_j)) \tag{7}$$

where $\beta > 0$ is a parameter with value fixed by the user, N_i denotes the local neighbourhood of the pixel $x_i (i \notin N_i)$, $l(x_i)$ and $l(x_j) (j \in N_i)$ represent the class label of the pixel x_i and its local neighbourhood, respectively, and the function I is defined as

$$I(l(x_i), l(x_j)) = \begin{cases} -w_{ij} & l(x_i) = l(x_j) \\ 0 & l(x_i) \neq l(x_j) \end{cases} \tag{8}$$

where w_{ij} is the spatial attraction between the centre pixel x_i and its neighbour pixel x_j instead of the traditional and equivalent value 1, and it can be calculated using the spatial attraction model as

$$w_{ij} = z(p_i) \times z(p_j) \times \frac{1}{R_{i,j}^2} \tag{9}$$

where i is the index of the centre pixel x_i, $j \in N_i\{j = 1, 2, ..., 8\}$ denotes the neighbourhood pixels of pixel x_i at 3×3 window as shown in figure 2(*a*), z represents the class label of the centre pixel x_i, and p_i and p_j are the fraction value of class z in pixel x_i and its neighbourhood pixels, which can be obtained from the membership probability of FCM. $R_{i,j}$ denotes the distance between pixel x_i and its neighbourhood pixels as shown in figure 2(*b*). More details about this issue can be found in Zhang *et al.* (in press).

There are some iterative algorithms to minimize the equation (5) like simulated annealing (SA), maximum a posterior margin (MPM), and iteration condition model (ICM) (Solberg *et al.* 1996). Considering the computational complexity, ICM is adopted in this paper to solve the equation (5). Since the cluster membership probability and the distances between the centre pixel and its neighbourhood pixels
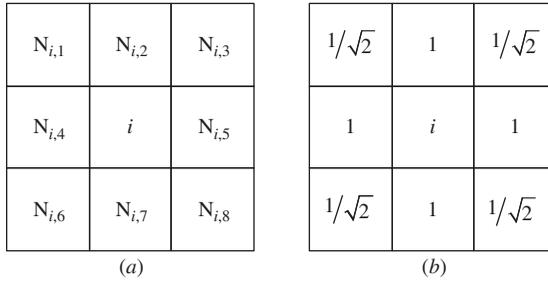
$N_{i,1}$	$N_{i,2}$	$N_{i,3}$		$1/\sqrt{2}$	1	$1/\sqrt{2}$
$N_{i,4}$	i	$N_{i,5}$		1	i	1
$N_{i,6}$	$N_{i,7}$	$N_{i,8}$		$1/\sqrt{2}$	1	$1/\sqrt{2}$
	(*a*)				(*b*)	

Figure 2. (*a*) Neighbourhood N_i of the centre pixel x_i, (*b*) distances between the centre pixel x_i and its neighbourhood N_i.

are introduced in MRF using the spatial attraction model, the risk of over-smooth results for the detailed change may be solved to a certain extent.

3. Experimental results and discussion

To evaluate the performance of the proposed approach, two remotely sensed data sets were tested by programming this approach in Matlab® 7.8 (MathWorks, Natick, MA, USA). Three indexes are used to assess the results: (1) miss detection (*MD*): the number of unchanged pixels in the changed detection map, incorrectly classified when compared to the ground reference map. The *MD* rate P_m is calculated by the ratio $P_m = MD/S_0 \times 100\%$, where S_0 is the total number of changed pixels counted in the ground reference map; (2) false alarm (*FA*): the number of changed pixels in the change detection map incorrectly classified when compared to the ground reference. The false detection rate P_f is described by the ratio $P_f = FA/S_1 \times 100\%$, where S_1 is the total number of unchanged pixels counted in the ground reference map; and (3) total error (*TE*): the total number of detection errors including both miss and false detections, which is the sum of the *FA* and the *MD*. Hence, the *TE* rate P_t is described by the ratio $P_t = (FA + MD)/(S_0 + S_1) \times 100\%$.

3.1. *Experiment on the data set 1*

The first data set was acquired by the Landsat 7 ETM+ sensor from the United States Geological Survey (USGS; Reston, VA, USA) in August 2001 (t_1) and August 2002 (t_2) in the Liaoning Province of China. A section (300 × 280 pixels) of the entire scene was cropped as the test site, and figures 3(*a*) and (*b*) show the band 4 of the both images, respectively. The t_1 image was registered and radiometrically corrected (i.e., histogram matching) to the t_2 image. Then the difference image was generated with all the bands except for the far-infrared band (band 6) using CVA method. Moreover, the ground reference map of changes was yielded manually and displayed in figure 3(*c*).

Figures 4(*a*)–(*f*) show the change detection results resulting from the multiresolution level set (MLS), MLS with Kittler algorithm (MLSK) (Bazi *et al.* 2010), FCM, the expectation maximization (EM), MRF (Bruzzone and Prieto 2000), and FCMMRF, respectively. In MLS and MLSK, the value of parameter μ is set to 0.2, and the values of parameter β in MRF and FCMMRF are set 1.8 and 4, respectively. As shown in figures 4 (*a*) and (*b*), MLS and MLSK produce change maps like the ground reference, while there is some "salt and pepper" noise in large change blocks (i.e., A region). EM and FCM produce much "salt and pepper" noise without considering contextual information as
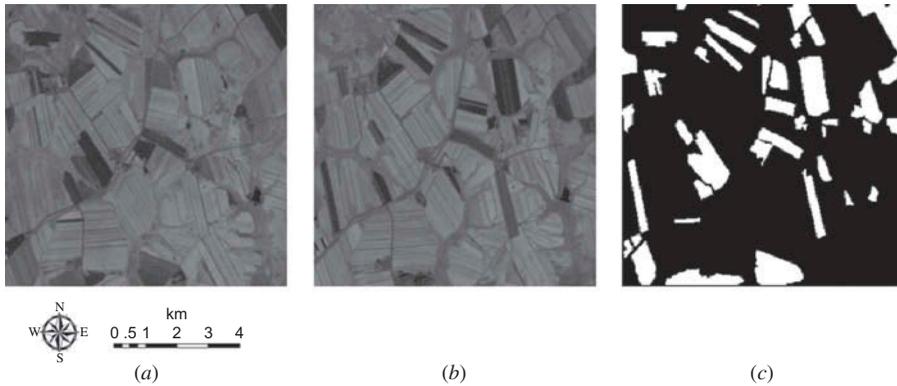
Figure 3. Band 4 of data set 1 (the centre coordinate: 48° 3′ N, 126° 8′ E) acquired by Landsat 7 ETM+ sensor in (*a*) August 2001 and (*b*) August 2002, (*c*) ground reference map.

presented in B region of figure 4(*c*) and A region of figure 4(*d*), respectively. Though figures 4(*d*) and (*f*) give more homogenous regions than other four methods in this paper, FCMMRF preserves detailed change information instead of over-smooth results occurring on boundary areas of the traditional MRF as shown in C region. Above all, the proposed FCMMRF yields the most close change map to the ground reference. The reason is that the spatial attraction is introduced as the adaptive weights for every pixel to control the proportion of spatial terms in MRF. Table 1 presents the accuracy comparisons of *FA*s, *MD*, and *TE*s between MLS, MLSK, EM, FCM, MRF, and FCMMRF. It is found that FCMMRF generates the most accurate result than other methods, because the cluster membership probability and distances between the centre pixel and its neighbourhoods are introduced in MRF using the spatial attraction model to control the boundary pixels. Considering the computing time, the proposed FCMMRF is slower than other methods because it combines FCM and MRF. Hence, when we want to obtain more accurate results, it is better to use FCMMRF, whereas, when the change maps need producing in shorter time, other methods should be exploited.

3.2. *Experiment on the data set 2*

The second data set is made up of two multispectral images of Alaska in July 1985 (t_1) and July 2005 (t_2) acquired by the Landsat 5 Thematic Mapper (TM) sensor from the USGS. A section (400 × 400 pixels) of the two scenes is selected for the experiment as presented band 4 of them in figures 5(*a*) and (*b*). The t_1 image was registered to the t_2 image, the histogram matching method was then applied to t_1 image by referencing t_2 image for the relative radiometric correction. The ground reference shown in figure 5(*c*) was created by the manual analysis of the two temporal images.

Figures 6(*a*)–(*f*) show the change detection results resulting from the MLS, MLSK (Bazi *et al.* 2010), EM, FCM, MRF (Bruzzone and Prieto 2000), and FCMMRF, respectively. In MLS and MLSK, the value of parameter μ is also set to 0.2, and the values of parameter β in MRF and FCMMRF are set 1.5 and 2.5, respectively. Seen from figures 6(*a*) and (*b*), MLS and MLSK produce change maps losing so much detailed change information (i.e., A region). Figure 6(*c*) contains much "salt and pepper" noise, because EM detects changes without considering contextual information (i.e., B region). Since many mixed pixels exist, FCM loses much detailed
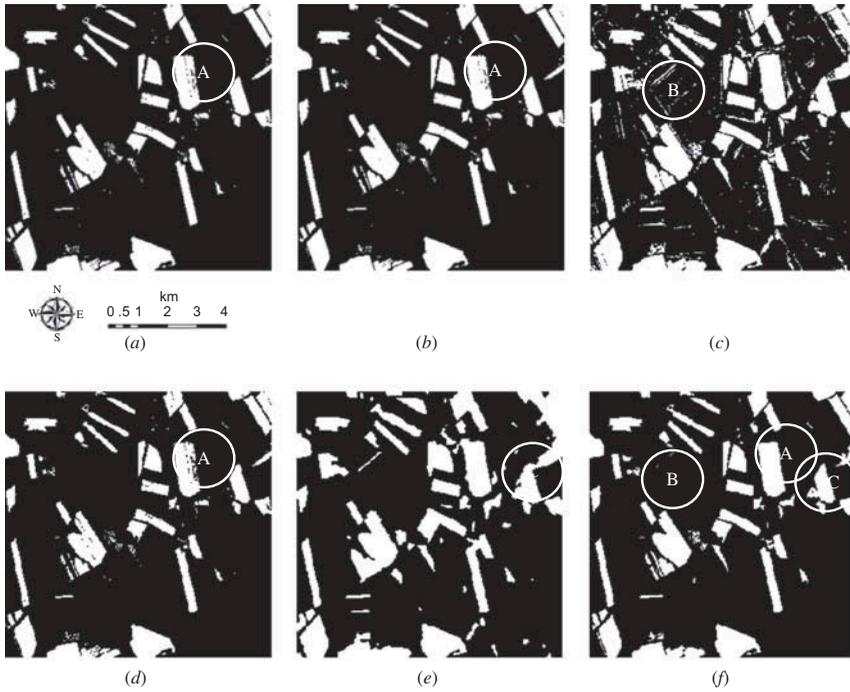
Figure 4.   Change detection results of data set 1 obtained by (*a*) MLS, (*b*) MLSK, (*c*) EM, (*d*) FCM, (*e*) MRF, and (*f*) FCMMRF model.

Table 1. Quantitative change detection results for the data set 1.

Methods	False alarms No. of pixels	P_f (%)	Missed detections No. of pixels	P_m (%)	Total errors No. of pixels	P_t (%)
MLS	722	1.1	3086	18.7	3808	4.5
MLSK	721	1.1	3054	18.6	3775	4.5
EM	5420	5.3	863	8.1	6283	7.5
FCM	669	1.0	3294	20.0	3963	4.7
MRF	4202	6.2	725	4.4	4927	5.8
FCMMRF	1230	1.8	2032	12.4	3262	3.8

information due to assigning pixels into the cluster of larger membership probability simply as shown in A region of figure 6(*d*). FCMMRF not only yields more homogenous regions but preserves detailed change information while MRF produces over-smooth result as shown in C region of figures 6(*d*) and (*f*). The reason is that the spatial attraction is introduced as the adaptive weights for every pixel to control the proportion of spatial terms in MRF. Table 2 lists the accuracy of *FA*s, *MD*, and *TE*s between MLS, MLSK, EM, FCM, MRF, and FCMMRF. As seen from table 2, since the cluster membership probability of FCM is added in MRF using the spatial attraction model, FCMMRF yields the highest change detection accuracy than other methods used in this paper. Because FCMMRF generates more accurate by combining FCM and MRF, it need more computing time than other methods used in this
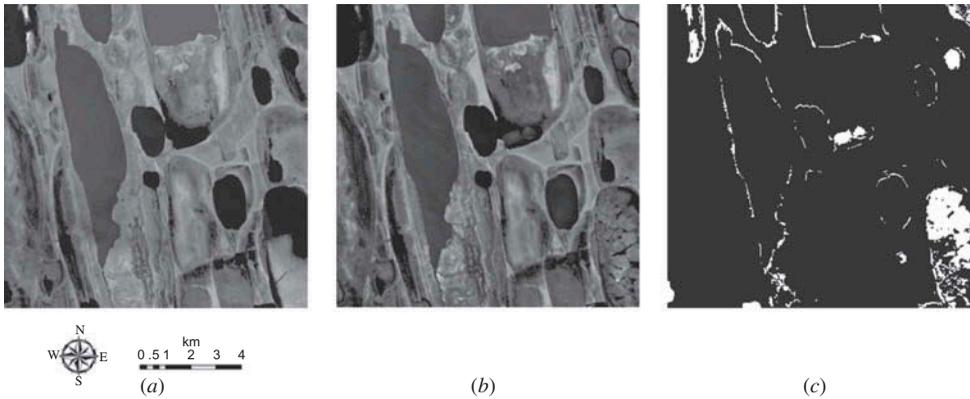
Figure 5. Band 4 of data set 2 (the centre coordinate: 70° 2′ N, 152° 8′ W) acquired by Landsat-5 TM sensor on (*a*) August 2001 and (*b*) August 2002, (*c*) ground reference map.
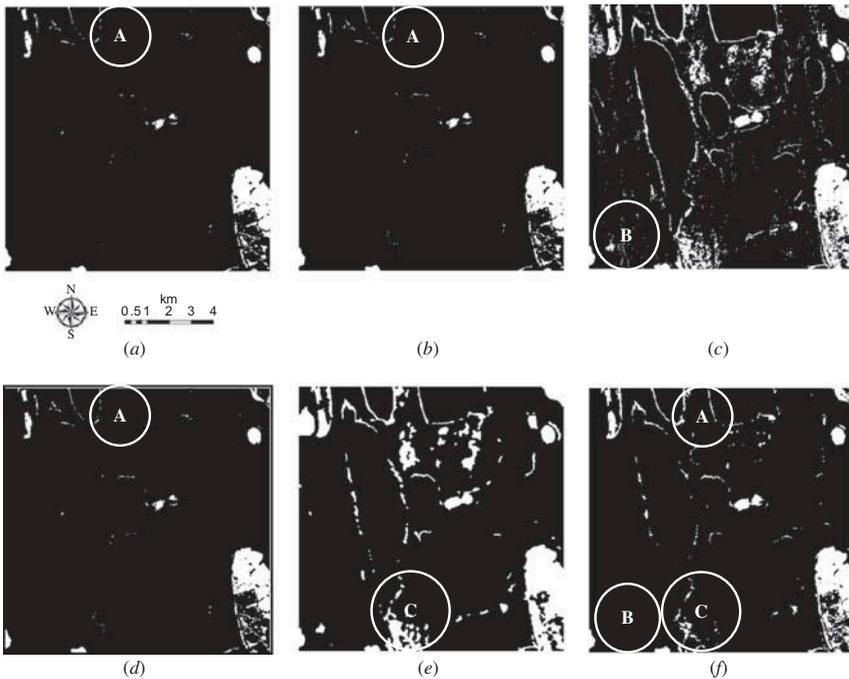

Figure 6. Change detection results of data set 2 obtained by (*a*) MLS, (*b*) MLSK, (*c*) EM, (*d*) FCM, (*e*) MRF, and (*f*) FCMMRF model.

paper. So it is better to use FCMMRF when more accurate results are required and other methods used in this paper should be selected for faster results.

4. Conclusions

In this paper, a novel change detection approach is proposed using FCM and MRF for remotely sensed images. First, FCM is applied to the difference image created by CVA method and the initial change map and cluster (changed and unchanged) membership probability are produced as the input data of the MRF incorporated the spatial

Table 2. Quantitative change detection results for the data set 2.

Methods	False alarms		Missed detections		Total errors	
	No. of pixels	P_f (%)	No. of pixels	P_m (%)	No. of pixels	P_t (%)
MLS	128	0.1	3639	37.4	3767	2.4
MLSK	138	0.1	3597	36.9	3735	2.3
EM	9323	6.2	107	1.1	9323	5.9
FCM	118	0.1	3595	36.9	3713	2.3
MRF	9042	6.0	449	4.6	9491	5.9
FCMMRF	1807	1.2	865	8.9	2672	1.6

attraction model. Then the cluster membership probability is introduced into MRF using the spatial attraction model, where the spatial attractions between the centre pixel and its neighbour pixels are computed as adaptive weights instead of the traditionally equivalent values. Finally, the final change map is generated through the improved MRF process. Two experiments were carried out to assesse the performance of the proposed FCMMRF. Through the comparisons with MLS, MLSK, EM, FCM and, MRF, FCMMRF not only obtains homogenous regions but preserves the detailed change information, and produces the most accurate change maps among these methods used in this paper. Hence, it is verified that FCMMRF is a more accurate approach to change detection for remotely sensed images.

Since FCMMRF produces more accurate results by combining FCM and MRF, it needs more computing time. If we want to generate more accurate change maps, it is better to select FCMMRF. In contrast, if we aim at yielding results in shorter time, other methods in this paper should be adopted. Additionally, how to determine the appropriate parameter β is worth the future work, and FCMMRF will be applied to other remotely sensed images type.

Funding

References

BAZI, Y., BRUZZONE, L. and MELGANI, F., 2005, An unsupervised approach based on the generalized Gaussian model to automatic change detection in multitemporal SAR images. *IEEE Transactions on Geoscience and Remote Sensing*, **43**, pp. 874–887.

BAZI, Y., MELGANI, F. and AL-SHARARI, H.D., 2010, Unsupervised change detection in multispectral remotely sensed imagery with level set methods. *IEEE Transactions on Geoscience and Remote Sensing*, **48**, pp. 3178–3187.

BEZDEK, J.C., EHRLICH, R. and FULL, W., 1984, FCM: the fuzzy c-means clustering algorithm. *Computers & Geosciences*, **10**, pp. 191–203.

BOVOLO, F. and BRUZZONE, L., 2005, A detail-preserving scale-driven approach to change detection in multitemporal SAR images. *IEEE Transactions on Geoscience and Remote Sensing*, **43**, pp. 2963–2972.

BOVOLO, F., BRUZZONE, L. and MARCONCINI, M., 2008, A novel approach to unsupervised change detection based on a semisupervised SVM and a similarity measure. *IEEE Transactions on Geoscience and Remote Sensing*, **46**, pp. 2070–2082.

BRUZZONE, L. and BOVOLO, F., 2013, A novel framework for the design of change-detection systems for very-high-resolution remote sensing images. *Proceedings of the IEEE*, **101**, pp. 609–630.

BRUZZONE, L. and PRIETO, D.F., 2000, Automatic analysis of the difference image for unsupervised change detection. *IEEE Transactions on Geoscience and Remote Sensing*, **38**, pp. 1171–1182.

CELIK, T. and MA, K.-K., 2010, Unsupervised change detection for satellite images using dual-tree complex wavelet transform. *IEEE Transactions on Geoscience and Remote Sensing*, **48**, pp. 1199–1210.

COPPIN, P., JONCKHEERE, I., NACKAERTS, K., MUYS, B. and LAMBIN, E., 2004, Digital change detection methods in ecosystem monitoring: a review. *International Journal of Remote Sensing*, **25**, pp. 1565–1596.

GHOSH, A., MISHRA, N.S. and GHOSH, S., 2011, Fuzzy clustering algorithms for unsupervised change detection in remote sensing images. *Information Sciences*, **181**, pp. 699–715.

HUANG, L.-K. and WANG, M.-J.J., 1995, Image thresholding by minimizing the measures of fuzziness. *Pattern Recognition*, **28**, pp. 41–51.

IM, J., JENSEN, J.R. and HODGSON, M.E., 2008, Optimizing the binary discriminant function in change detection applications. *Remote Sensing of Environment*, **112**, pp. 2761–2776.

LIU, D., SONG, K., TOWNSHEND, J.R. and GONG, P., 2008, Using local transition probability models in Markov random fields for forest change detection. *Remote Sensing of Environment*, **112**, pp. 2222–2231.

LU, D., MAUSEL, P., BRONDÍZIO, E. and MORAN, E., 2004, Change detection techniques. *International Journal of Remote Sensing*, **25**, pp. 2365–2401.

MARCHESI, S., BOVOLO, F. and BRUZZONE, L., 2010, A context-sensitive technique robust to registration noise for change detection in VHR multispectral images. *IEEE Transactions on Image Processing*, **19**, pp. 1877–1889.

MELGANI, F. and BAZI, Y., 2006, Markovian fusion approach to robust unsupervised change detection in remotely sensed imagery. *IEEE Geoscience and Remote Sensing Letters*, **3**, pp. 457–461.

MOSER, G. and SERPICO, S.B., 2009, Unsupervised change detection from multichannel SAR data by Markovian data fusion. *IEEE Transactions on Geoscience and Remote Sensing*, **47**, pp. 2114–2128.

RADKE, R.J., ANDRA, S., AL-KOFAHI, O. and ROYSAM, B., 2005, Image change detection algorithms: a systematic survey. *IEEE Transactions on Image Processing*, **14**, pp. 294–307.

SHI, W. and HAO, M., 2013, Analysis of spatial distribution pattern of change-detection error caused by misregistration. *International Journal of Remote Sensing*, **34**, pp. 6883–6897.

SOLBERG, A.H., TAXT, T. and JAIN, A.K., 1996, A Markov random field model for classification of multisource satellite imagery. *IEEE Transactions on Geoscience and Remote Sensing*, **34**, pp. 100–113.

TARABALKA, Y., FAUVEL, M., CHANUSSOT, J. and BENEDIKTSSON, J.A., 2010, SVM-and MRF-based method for accurate classification of hyperspectral images. *IEEE Geoscience and Remote Sensing Letters*, **7**, pp. 736–740.

TSO, B. and OLSEN, R.C., 2005, A contextual classification scheme based on MRF model with improved parameter estimation and multiscale fuzzy line process. *Remote Sensing of Environment*, **97**, pp. 127–136.

WANG, F., WU, Y., ZHANG, Q., ZHANG, P., LI, M. and LU, Y., 2013, Unsupervised change detection on SAR images using triplet Markov field model. *IEEE Geoscience and Remote Sensing Letters*, **10**, pp. 697–701.

WANG, X. and WANG, H., 2004, Markov random field modeled range image segmentation. *Pattern Recognition Letters*, **25**, pp. 367–375.

YETGIN, Z., 2012, Unsupervised change detection of satellite images using local gradual descent. *IEEE Transactions on Geoscience and Remote Sensing*, **50**, pp. 1919–1929.

ZHANG, H., SHI, W., WANG, Y., HAO, M. and MIAO, Z., In press, Spatial attraction based Markov random field approach for classification of high spatial resolution multispectral imagery. *IEEE Geoscience and Remote Sensing Letters*, doi:10.1109/LGRS.2013.2268968.